AGU PUBLICATIONS

JGR

Journal of Geophysical Research: Oceans

RESEARCH ARTICLE

10.1002/2017JC013049

Turbulent mixing within the Kuroshio in the Tokara Strait

Eisuke Tsutsumi[1], Takeshi Matsuno[1], Ren-Chieh Lien[2], Hirohiko Nakamura[3], Tomoharu Senjyu[1], and Xinyu Guo[4]

[1]Research Institute for Applied Mechanics, Kyushu University, Fukuoka, Japan, [2]Applied Physics Laboratory, University of Washington, Seattle, Washington, USA, [3]Faculty of Fisheries, Kagoshima University, Kagoshima, Japan, [4]Center for Marine Environmental Studies, Ehime University, Matsuyama, Japan

Key Points:
- Direct measurements of turbulence were conducted in the Tokara Strait where many seamounts and islands exist within the Kuroshio
- Analyses suggest vertical diffusivity could have been elevated to 10^{-1} m^2 s^{-1} around a shallow seamount with which the Kuroshio interacts
- Flow-topography interaction and associated mixing processes are key to modeling the downstream evolution of the Kuroshio water properties

Correspondence to:
E. Tsutsumi,
tsutsumi@riam.kyushu-u.ac.jp

Citation:
Tsutsumi, E., T. Matsuno, R.-C. Lien, H. Nakamura, T. Senjyu, and X. Guo (2017), Turbulent mixing within the Kuroshio in the Tokara Strait, *J. Geophys. Res. Oceans*, *122*, 7082–7094, doi:10.1002/2017JC013049.

Received 2 MAY 2017
Accepted 10 AUG 2017
Accepted article online 25 AUG 2017
Published online 4 SEP 2017

Abstract Turbulent mixing and background current were observed using a microstructure profiler and acoustic Doppler current profilers in the Tokara Strait, where many seamounts and small islands exist within the route of the Kuroshio in the East China Sea. Vertical structure and water properties of the Kuroshio were greatly modified downstream from shallow seamounts. In the lee of a seamount crest at 200 m depth, the modification made the flow tend to shear instability, and the vertical eddy diffusivity is enhanced by nearly 100 times that of the upstream site, to $K_\rho \sim O(10^{-3})$–$O(10^{-2})$ m^2 s^{-1}. A one-dimensional diffusion model using the observed eddy diffusivity reproduced the observed downstream evolution of the temperature-salinity profile. However, the estimated diffusion time-scale is at least 10 times longer than the observed advection time-scale. This suggests that the eddy diffusivity reaches to $O(10^{-1})$ m^2 s^{-1} in the vicinity of the seamount. At a site away from the abrupt topography, eddy diffusivity was also elevated to $O(10^{-3})$ m^2 s^{-1}, and was associated with shear instability presumably induced by the Kuroshio shear and near-inertial internal-wave shear. Our study suggests that a better prediction of current, water-mass properties, and nutrients within the Kuroshio requires accurate understanding and parameterization of flow-topography interaction such as internal hydraulics, the associated internal-wave processes, and turbulent mixing processes.

1. Introduction

The Kuroshio, which is a western boundary current in the subtropical North Pacific, carries a large amount of heat, salt and momentum from the low- to mid- latitude ocean. The Kuroshio has a potential impact on biogeochemical processes along its path through nutrient transport [*Liu et al.*, 2014; *Guo et al.*, 2013; *Kodama et al.*, 2014]. There are horizontal and vertical aspects to nutrient transport within the Kuroshio; the latter is mainly caused by turbulent mixing [e.g., *Guo et al.*, 2013]. The Kuroshio affects turbulence processes through propagation and breaking of internal tidal and inertial waves by its current and geostrophic shears [e.g., *Alford et al.*, 2015; *Nagai et al.*, 2015]. Turbulence may modify the temperature and salinity of the Kuroshio through mixing with surrounding water, incorporating properties of the water-mass in each area along its route from the origin (Philippine sea-Luzon Strait) to south of Japan [*Nakamura et al.*, 2013; *Andres et al.*, 2015; *Lien et al.*, 2015; *Kida et al.*, 2015] as well as its marginal shelf and inner seas [e.g., *Yanao and Matsuno*, 2013; *Tsutsumi and Guo*, 2016]. Therefore, it is vital to investigate turbulent mixing processes within the Kuroshio to understand physical and biogeochemical processes in the western North Pacific.

Besides the surface-induced turbulent mixing, the most likely driving mechanism of mixing within the Kuroshio is flow-topography interactions. Previous studies on sub-tidal flow interaction with topography reported strong turbulence in hydraulic jumps [*St. Laurent and Thurnherr*, 2007; *Alford et al.*, 2013; *Alford and MacCready*, 2014; *Nishina et al.*, 2016] and lee waves [*Nikurashin and Ferrari*, 2010a; *Sheen et al.*, 2013; *Waterman et al.*, 2013]. Such hydraulic jumps can cause huge vertical eddy diffusivity, $K_\rho = O(10^{-2})$–$O(10^{-1})$ m^2 s^{-1} [*St. Laurent and Thurnherr*, 2007; *Alford et al.*, 2013; *Nishina et al.*, 2016]. Internal tides are another candidate for promoting mixing. At the margin of the South China Sea, such as in the Luzon Strait where strong internal tides are generated, internal wave propagation and breaking and their relation to the Kuroshio and mesoscale and submesoscale variabilities have been studied extensively [*Klymak et al.*, 2011; *Rainville et al.*, 2013; *Lien et al.*, 2013; *Alford et al.*, 2015]. Tidal currents can also produce hydraulic jumps and lee waves as they interact with topography [*Legg and Klymak*, 2008; *Nakamura et al.*, 2010; *Mohri et al.*, 2010; *Gregg and Klymak*, 2014] and cause enhanced eddy diffusivity of $O(10^{-2})$–$O(10^{-1})$ m^2 s^{-1} [*Klymak and Gregg*, 2004; *Alford et al.*, 2011].

Strong turbulent mixing due to internal waves and Kuroshio interaction with topography has been measured or inferred along the path of the Kuroshio. *Rainville and Pinkel* [2004] observed high-wavenumber internal waves trapped by the horizontal shear of the Kuroshio near the shelf break of the East China Sea (ECS) and within the current core of the Kuroshio west of Kyushu Island, Japan. The turbulent energy dissipation rate ε, estimated using fine-scale parameterization, was 0.5–1.5 $\times 10^{-8}$ W kg^{-1}. Near the shelf break of the ECS, *Matsuno et al.* [2005] measured the dissipation rate using a microstructure profiler. They found an increase in dissipation rate in the thermocline, $\varepsilon = O(10^{-8})$–$O(10^{-7})$ W kg^{-1}, and discussed its relation to observed high-wavenumber M_2 internal tide around the shelf edge. This dissipation rate was similar to the estimate by *Rainville and Pinkel* [2004]. At the Tokara Islands chain within the Kuroshio south of Kyushu Island, Japan, *Hasegawa et al.* [2008] reported formations of cold water and estimated the turbulent dissipation, $\varepsilon = 0.2$–1.1×10^{-4} W kg^{-1}, which was more than two orders of magnitude greater than the reported value at the ECS shelf edge. *Chang et al.* [2013] observed similar cold eddy formation in the wake of Green Island, east of Taiwan within the Kuroshio. They also estimated an energy dissipation rate of $\varepsilon = O(10^{-7})$–$O(10^{-5})$ W kg^{-1}. Recently, *Chang et al.* [2016] reported generation of extremely strong turbulence over a seamount within the Kuroshio east of Taiwan. Kelvin-Helmholtz billows were generated as a result of the Kuroshio interacting with a seamount, leading to enhanced turbulent dissipation rates, $O(10^{-6})$–$O(10^{-3})$ W kg^{-1}. From these studies, it is clear that the Kuroshio-topography interaction plays an important role in producing strong turbulent mixing.

Here, we present the observational evidence of strong turbulent mixing in the Tokara Strait. The Tokara Strait is the passage and the marginal area between Yakushima and Amami-oshima Islands where the Kuroshio exits from the ECS to the northwestern Pacific (Figures 1a and 1b). The strait is distinctively characterized by many abrupt topographic features such as seamounts and small islands, and they are shallower than 300 m depth in the path of Kuroshio, as shown by green contours in Figure 1. The depths of the abrupt topography in the Tokara Strait are comparable to or shallower than the typical depth of the base of the Kuroshio flow in the ECS, 400–500 m [e.g., *Guo et al.*, 2013]. We define the Kuroshio path based on the

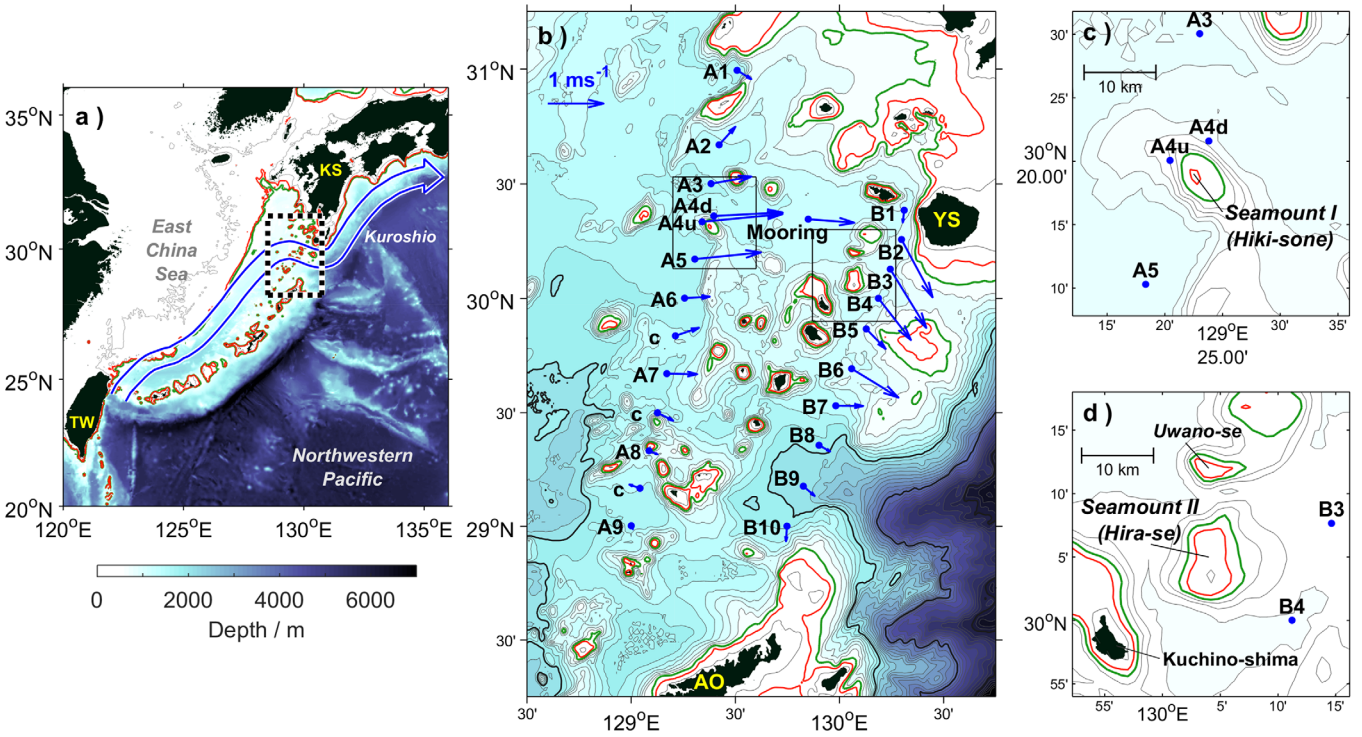

Figure 1. Map showing the geography of the Kuroshio in East China Sea (ECS) and our experimental site in the Tokara Strait. (a) A typical pathway of the Kuroshio from east of Taiwan (TW) to the east of Kyushu (KS) Island. Location of the Tokara Strait is indicated by dashed-line box. (b) Location of microstructure stations in the Tokara Strait (blue dots). Microstructure surveys were conducted in two meridional sections A and B across the Kuroshio. A chain of islands and seamounts are present between sections A and B. Blue arrows show temporal averages of velocities at 24 m depth measured by shipboard ADCP. Yakushima Island and Amami-oshima Island are indicated by "YS" and "AO," respectively. (c, d) Enlarged views of two seamounts. In each plot, red and green contours represent 200- and 300 m isobaths, respectively.

average of the Kuroshio axis position data set 1955–2006 by the Japan Hydrographical Association, following previous studies [e.g., *Nakamura et al*., 2012]. The Kuroshio almost always flows through the section between Yakushima and Amami-oshima Islands ('YS' and 'AO' in Figure 1b, respectively). The Tokara Strait is therefore the most likely area where the Kuroshio interacts with topography at the margin of the ECS. Observational evidence of strong turbulence in this region is limited to a few studies [e.g., *Hasegawa et al*., 2008].

The Tokara Strait is also one of the major generation sites of internal tides in the North Pacific. *Niwa and Hibiya* [2004] estimated 9.3 GW of semidiurnal (M_2) internal tide energy is converted from barotropic tide at the Tokara Strait, while *Varlamov et al*. [2015] estimated it as 3.8 GW. These values are significant compared with the conversion rate at the energetic Luzon Strait. For M_2: 14 GW [*Niwa and Hibiya*, 2004], 16 GW [*Kerry et al*., 2014] and 11 GW [*Varlamov et al*., 2015]; for M_2+S_2: 11 GW [*Jan et al*., 2008]; or for four major constituents, 24 GW [*Alford et al*., 2011]. Numerical simulation indicates that a significant fraction of the internal tide energy is dissipated locally and therefore, turbulence generation is expected in the Tokara Strait [*Niwa and Hibiya*, 2004]. To date, almost no observation of internal tides and the associated turbulence in the Tokara Strait has been reported.

Identifying the locations, strengths and driving mechanism of vertical mixing within the Kuroshio is important for understanding the water-mass modification, material transport and biological productivity in its marginal area. As noted above, the Tokara Strait is the most likely spot to produce energetic turbulent mixing in the ECS because of abrupt topography, tides, and the Kuroshio, although they are poorly understood. In the following, we report a systematic survey of microstructure, currents and water properties in the Tokara Strait for the first time.

2. Experiment

An observational experiment was conducted on board *T/V Kagoshima-maru* to study turbulent mixing and water-mass modification along and across the Kuroshio in the Tokara Strait in November 2015. This experiment was motivated by a need for a better understanding of the spatial and temporal variations of microstructure turbulence and interactions among the Kuroshio, tidal currents and bottom topography over the entire strait. A mooring with an up-ward looking Teledyne RDI 75 kHz Long Ranger ADCP was deployed at a location where the water depth is 650 m in the pathway of the Kuroshio. The moored ADCP obtained an ensemble of 27-ping data every 1 min (2.22 s ping rate) with a vertical bin size of 8 m for 6 days from 0830JST (Japan Standard Time: UTC+9 h) on 15 November to 1200JST on 21 November.

During the mooring observation period, we carried out measurements of turbulence, currents, temperature and salinity using a loosely tethered, free-falling microstructure profiler, TurboMAP-L (JFE Advantech Co.), shipboard 75-kHz Ocean Surveyor ADCP (RDI) and shipboard SBE-9p CTD (Sea-bird Electronics Inc.). Bin size and ensemble interval of the shipboard ADCP were 16 m and approximately 10 min, respectively. These observations were made at 19 stations along the two transects across the Kuroshio (Line A and B: Figure 1b). These two transects were chosen to capture along- and cross-stream variabilities of turbulence and water properties in the Kuroshio. At each station shown in Figure 1b, double TurboMAP-L casts and single SBE-9p cast were performed, except for Stn.A4u/d, stations labeled by 'c', and the mooring site. Double TurboMAP-L casts and single TurboMAP-L/SBE-9p cast were made at Stn.A4u and A4d, respectively. Note that subscripts 'u' and 'd' mean upstream and downstream of a seamount, respectively (Figure 1c). At stations 'c', a single SBE-9p cast was performed. At the mooring site, a series of TurboMAP-L and SBE-9p casts were made at nearly 2 h intervals for 25 h starting at 0630 JST on 20 November.

The TurboMAP-L measures turbulent shear and temperature fluctuations using two orthogonally-orientated shear probes and a fast-response thermistor (FP07), respectively. All microstructure sensors sample at 512 Hz. Conductivity, temperature and pressure are measured by standard CTD sensors at 64 Hz. The TurboMAP-L falls from surface to 500–600 m depth, not reaching to the sea floor, at a speed of $\sim$0.6 m s^{-1}. At some stations where the vertical shear of horizontal velocity was too strong such as Stn.A4d and Stn.B4, the profiler stopped descending at half of the targeted depth because of a limited cable length.

The surface wind, measured by shipboard meteorological sensors, was moderate during most of the observational period. The wind speed increased to $>$10 m s^{-1} for 1.5 days after midnight on 18 November because of the passage of a low-pressure system (figure not shown). The poor sea state interrupted our

measurements at Stn.B7 for 1/2 day from the afternoon on 18 November. The atmospheric disturbances did not seem to have significant effect on oceanic conditions below the surface mixed layer.

The dissipation rate of turbulent kinetic energy, ε, is computed from turbulent shear by fitting its wavenumber spectrum to an empirical spectrum [*Nasmyth*, 1970] and integrating the shear spectrum in wavenumber space for each 1024-point segment (equivalent to ~1.2 m in vertical) with half overlapping. Profiles of ε were then interpolated onto a 1 m vertical grid. Potential temperature T and salinity S were calculated using the in-situ temperature, conductivity, and pressure after adjusting the response lag of the thermistor relative to the conductivity sensor to minimize salinity spikes. Buoyancy frequency, $N^2 = -(g/\rho_0)(\partial\bar{p}/\partial z)$ is calculated from potential density ρ where g is the gravitational acceleration, ρ_0 is a reference density (1025 kg m^{-3}) and $\bar{p}$ is the mean density, which is sorted to be gravitationally stable. The vertical displacement of a water parcel due to a turbulent fluctuation d is computed as $d = z(\rho) - z(\bar{p})$. The vertical eddy diffusivity is estimated by Osborn's method, $K_\rho = \Gamma\varepsilon N^{-2}$, with a constant mixing efficiency $\Gamma = 0.2$ [*Osborn*, 1980].

The dissipation rate and eddy diffusivity are also estimated based on the *Thorpe* scale method, $\varepsilon_T = 0.64 L_T^2 N^3$ and $K_{\rho T} = \Gamma\varepsilon_T N^{-2}$, where L_T is the Thorpe scale defined as the root-mean-square of d within each overturn [*Thorpe*, 1977; *Dillon*, 1982]. We estimated the vertical turbulent heat flux $J_q = \rho_0 c_p K_T (\partial T/\partial z)$ where c_p is the heat capacity of seawater (4×10^3 J kg^{-1}°C^{-1}) and K_T is the vertical eddy diffusivity of heat. Positive values of J_q represent downward heat transport. In this study, we assume $K_T = K_\rho$.

3. Results

3.1. Spatial Variation of Currents and Turbulence

Figure 1b shows surface velocities at 24 m depth from the shipboard ADCP. During the experimental period, the core of the Kuroshio, with a typical speed of ~1 m s^{-1} and width of ~50 km, flowed eastward at Stn.A3–A5 and turned south-eastward at Stn.B2–B4. This pathway was characterized as the northern mode by *Nakamura et al*. [2003] who reported that the Kuroshio exhibits a bi-modal (northern and southern modes) pathway in the Tokara Strait. Significant eastward and southeastward currents with magnitude of 0.5–1 m s^{-1} were also observed around A7 and B6, respectively. These are probably branches of the Kuroshio separated by the Tokara Islands and related to a double-core velocity structure in the Kuroshio reported in the area south of Yakushima Island (Figure 1b) [*Feng et al*., 2000; *Oka and Kawabe*, 2003; *Nakamura et al*., 2003].

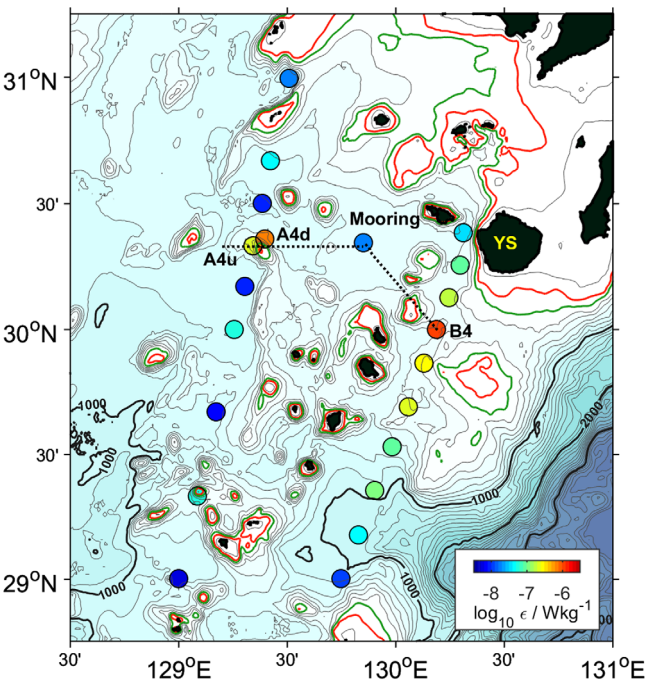

Figure 2. Depth-averaged turbulent dissipation rate in the main pycnocline shown by colored circles. Depth-averaging was performed between the base of the surface mixed layer and the bottom of profile, typically 500–600 m depth. Dissipation rates are also averaged using two casts in each station, except for Station A4d and the mooring station where they were taken from a single profile and averaged for 25 h (or 23 casts), respectively. Isobaths are the same as Figure 1b. Dotted lines represent a selected section along the Kuroshio core shown in Figure 3.

Depth-averaged turbulent dissipation rate shows the spatial variation in turbulence strength in the Tokara Strait (Figure 2). Depth-averaging was performed from below the base of the surface mixed layer, defined as the depth where potential density exceeds 0.01 σ_θ relative to its shallowest value, down to the bottom of the profile (typically 500–600 m depth). Therefore, this average represents mean turbulence strength in the main pycnocline. The depth-averaged turbulent dissipation rates are typically $O(10^{-8})$–$O(10^{-7})$ W kg^{-1}. The turbulent dissipation rates are significantly elevated to 2.8×10^{-7}

W kg^{-1} at A4d and 1.1 $\times$ 10^{-6} W kg^{-1} at B4 in the Kuroshio core. This observed strong turbulence is likely to have originated from interaction between the Kuroshio and the complex topography, namely Hiki-sone Seamount at A4 and Hira-se Seamount near B4 (Figures 1c and 1d). Detailed analyses of the Kuroshio-topography interaction will be presented in the next subsection, in connection with the vertical shear of the Kuroshio velocity enhanced by seamounts.

3.2. Vertical Structure of Currents, Shear Instability, and Turbulence

Downstream evolution of the velocity structure, stratification and turbulence strength along the Kuroshio core highlights the impact of the topography on the Kuroshio current and turbulence (Figure 3). Here, we

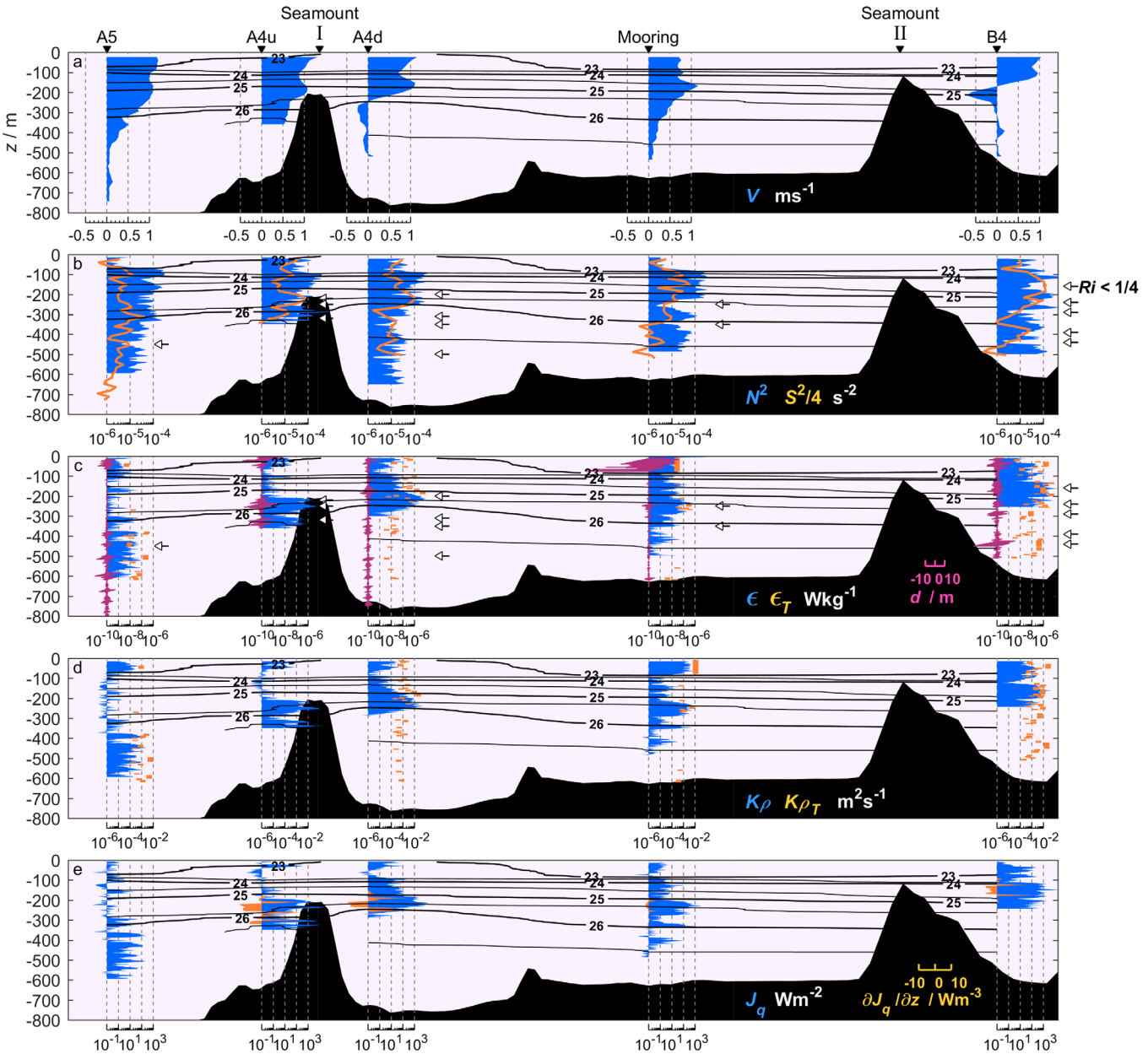

Figure 3. Vertical profiles of flow velocity, stratification, and turbulence at the stations in the pathway of the Kuroshio core: A5, A4u/d, mooring site and B4. (a) along-stream velocity V (positive in the downstream direction), (b) Buoyancy frequency squared N^2 (blue shading) and vertical shear squared divided by a factor of 4, $S^2/4$ (orange line), (c) turbulent dissipation rate ε (blue shading) and parcel displacement d (purple line, the scale is given at the lower right), (d) vertical eddy diffusivity K_ρ (blue shading), (e) vertical turbulent heat flux J_q defined as positive downward (blue shading) and its vertical divergence $\partial J_q/\partial z$ (orange line, the scale is given at the lower right). Solid lines indicate isopycnals at an interval of 0.5 σ_θ. Parcel displacements are calculated from shipboard CTD data except for A4u. Profiles at the mooring site are from the last cast of 25 h measurement. Horizontal arrows in Figures 3b and 3c represent the depths where gradient Richardson number around the pycnocline is smaller than 1/4. Orange lines in Figures 3c and 3d show estimates of ε and K_ρ by the Thorpe scale method, ε_T and $K_{\rho T}$, respectively. In each plot, bottom topography along the dotted line marked in Figure 2 is schematically shown by the black shade.

focus on two shallow seamounts in the Kuroshio path, Hiki-sone Seamount (hereinafter, Seamount I) adjacent to Stns.A4u/A4d and Hira-se Seamount (hereinafter, Seamount II) about 15 km upstream of B4 (Figures 1c and 1d). Profiles at Stn.A5 and the mooring site, which are located far from any significant abrupt topography, are presented to illustrate the undisturbed state of the Kuroshio and turbulence upstream of the seamount.

At Stn.A5, flow is characterized by the Kuroshio with 0.5–1 m s^{-1} speed and 300 m thickness (Figure 3a). These features correspond to the typical values of the Kuroshio in the ECS [*James et al*., 1999; *Andres et al*., 2008; *Guo et al*., 2012]. Gradient Richardson number, $Ri = N^2S^{-2}$, is larger than 1/4 at most depths of the water column and turbulent dissipation rate is $O(10^{-10})$–$O(10^{-8})$ W kg^{-1} (Figures 3b and 3c). At this site, flow is free from topographic effects and therefore the turbulence is considered to represent a typical value in the Kuroshio in the ECS.

At Stn.A4d, a few kilometers downstream of Seamount I, the magnitude of the Kuroshio sharply weakens below the 200 m depth and the flow reverses below 250 m, while the flow remains almost the same as that in the upper 200 m layer at A5. Such a velocity drop cannot be found at A4u, a few kilometers upstream of Seamount I. Vertical shear is enhanced in the lower pycnocline at A4d, and the Richardson number is correspondingly smaller than 1/4 at several depths below 200 m (indicated by white arrows in Figures 3b and 3c). Layers of shear instability coincide with layers of strong turbulent dissipation reaching $O(10^{-7})$–$O(10^{-6})$ W kg^{-1}, indicating that shear instability is the driving mechanism for the energetic turbulence. Significant density overturning at order of $O(1)$–$O(10)$ m is observed in the small *Ri* layer (Figure 3c, purple lines).

At the mooring site, the eastward Kuroshio current again penetrates deeper than 300 m, with a speed of 0.3–0.8 m s^{-1} (Figure 3a). In Figure 3, we show a typical profile of 25 h TurboMAP-L casts. Temporal evolutions of currents and turbulence at the mooring site are described later. Turbulent dissipation rate and eddy diffusivity have a peak reaching $\varepsilon = O(10^{-7})$ W kg^{-1} and $K_\rho = O(10^{-3})$ m^2 s^{-1}, respectively at 250 m depth ($\sim$25.6 σ_θ isopycnal) where is *Ri* is smaller than 1/4 (Figures 3c and 3d). Overall, vertical diffusion at the mooring site is weaker than at A4d, but it is significant at 200–300 m depth.

At Stn.B4, located 50 km downstream from the mooring site and 15 km downstream from Seamount II, vertical profiles of current and turbulence change drastically. The eastward Kuroshio current is limited to the upper 200 m and a strong subsurface counter-current with a speed of 0.5 m s^{-1} appears below the Kuroshio (Figure 3a). This velocity structure leads to a thick and enhanced shear layer in the upper pycnocline in 130–200 m depths, corresponding to the shallowest depth of Seamount II, $\sim$150 m depth (Figure 3b). Within this layer, the flow is in favor of shear instability, $Ri < 1/4$, and the turbulent dissipation rate is elevated, $\varepsilon = O(10^{-6})$ W kg^{-1}, which is 100–1000 times that in the same density layer at the upstream mooring site (Figure 3c). Although microstructure measurement stopped at 250 m depth at B4, large vertical overturns *d*, observed by the shipboard CTD, with small Richardson numbers suggest the occurrence of elevated turbulence in the deeper layers, e.g., 300 and 450 m depths (Figure 3c). An estimation based on the Thorpe scale method, which nearly agrees with the microstructure estimate, indicates that turbulent dissipation is indeed enhanced in the deeper layer at B4, $\varepsilon = O(10^{-7})$ W kg^{-1} at 400–500 m (orange lines in Figure 3c). This value is comparable to high dissipation rates measured at around 150 m depth at B4. Strong vertical eddy diffusivity reaching $K_\rho = O(10^{-3})$–$O(10^{-2})$ m^2 s^{-1} is observed downstream of Seamount II (Figure 3d). The vertical heat flux J_q is elevated in the pycnocline near and downstream of the seamounts (Figure 3e). Its vertical divergence $\partial J_q/\partial z$ has a magnitude of 5–10 W m^{-3} at A4u/d and B4, which is 1000–10,000 times larger than those upstream of seamounts. Such vertical divergence may lead to a temperature evolution of 0.1–0.2°C in 1 day. The observed vertical mixing is expected to result in strong water-mass modification.

We speculate that the observed elevated turbulence within the Kuroshio downstream of seamounts is due to the shear instability resulting from the blocking effect on the Kuroshio deep-flow, similar to that reported by *Chang et al*. [2016]. This hypothesis is supported by the observational fact that the vertical shear of the Kuroshio increases at depths similar to the top summits of both seamounts: shear peaks appear at 200 m depth near Seamount I and at 150 m depth downstream of Seamount II (Figure 3b). Flow over topography may be characterized by the topographic Froude number $Fr_t = U_0/(Nh_0)$, where U_0 is the upstream velocity and h_0 topography height [*Baines*, 1995; *Klymak et al*., 2010]. At Seamount II, $U_0 = 0.5$ m s^{-1}, $N = 10^{-2}$ s^{-1}, and $h_0 = 500$ m yields $Fr_t^{-1} = Nh_0/U_0 = 10$. The large inverse Froude number suggests that the upstream water is partially blocked by the topography, as evident in our observations, and lee waves are generated

[*Baines*, 1995; *Klymak et al*., 2010]. The Kuroshio-topography interaction probably triggers internal hydraulics and internal lee waves. Nonlinear steepening of the lee waves probably leads to wave breaking and turbulent mixing. We expect turbulent mixing in the vicinity of the seamount would be much stronger than at our observational sites, which will be demonstrated later.

3.3. Temporal Variations of Currents and Turbulence at the Mooring Site

At the mooring site, we observed modulation of the Kuroshio flow and turbulence by tides and waves. Figures 4a–4e show the temporal variations of barotropic tidal velocities, baroclinic tidal velocities, and time-averaged velocity. Here, tidal velocity is defined as an anomaly from time-average. Barotropic and baroclinic tidal velocities are calculated as depth-averaged tidal velocity and as an anomaly from the depth-averaged tidal velocity, respectively.

Barotropic velocity during the 25 h of profiling is mainly semidiurnal and typically has a magnitude of 0.1 m s^{-1} (Figure 4a). Baroclinic tidal currents have a magnitude of 0.1–0.3 m s^{-1} which are comparable to time-averaged velocities, induced mainly by the Kuroshio, with a magnitude of $\sim$0.5 m s^{-1}. The baroclinic currents have a high-vertical-wavenumber structure, as well as a low-mode semidiurnal one, creating time-evolving enhanced shear layers (Figure 4f). The turbulent dissipation rate is elevated to $O(10^{-7})$ W kg^{-1}, especially within strong shear layer at 200–300 m depths during the latter half of the profiling period. This strong turbulence is clearly associated with small Richardson numbers within the enhanced shear layer ($Ri < 1/4$, Figure 4g). Vertical diffusivity is similarly elevated at 200–300 m depths to $O(10^{-4})$–$O(10^{-2})$ m^2 s^{-1} (Figure 4h).

In the enhanced shear layer at 200–300 m depths, vertical movement of isopycnals (e.g., 25.0 and 25.5 σ_θ) is diurnal rather than semidiurnal (Figure 4). The enhanced shear and turbulence in the latter half of the profiling period also imply diurnal variability. At the mooring site (30.46°N), the inertial frequency (0.9973 cpd: cycle per day) is nearly same as the diurnal frequency (K1 constituent: 1.0029 cpd).

Previous numerical model simulations showed that strong semi-diurnal internal tides are generated in the Tokara Strait and suggested that they can lead to local mixing [e.g., *Niwa and Hibiya*, 2004]. However, our observation suggests that strong turbulence is related to diurnal/inertial baroclinic motion rather than a semi-diurnal one. *Rainville and Pinkel* [2004] and *Nagai et al*. [2015] indicated that elevated turbulence in the Kuroshio is related to high-wavenumber near-inertial internal wave shear. We speculate that near-inertial waves play an important role in the modulation of the vertical shear and turbulence strength observed at the mooring site, although the hypothesis cannot be demonstrated from our limited observations.

The relatively weak turbulence strength at the mooring site suggests that internal tides may have, at most, secondary impacts on turbulent mixing in the Tokara Strait [*Niwa and Hibiya*, 2004]. The turbulent mixing in Tokara Strait is driven primarily by the Kuroshio deep current interacting with the abrupt topography. In the following discussion, we focus our scope on the turbulent mixing and water-mass modification around the Seamount II.

4. Discussion

4.1. *T-S* Transformation by Vertical Mixing Along the Kuroshio Pathway

Turbulent mixing can modify the *T-S* properties of water masses along the Kuroshio. Here, we examine *T-S* evolution upstream and downstream of Seamount II using observations at the mooring site and B4, respectively. Figure 5 shows *T-S* relation at the mooring site and B1–B8. The 25 h-averaged *T-S* properties at the mooring site represent typical Kuroshio water (black dots in Figure 5). Water masses at B5–B8 (yellow-green dots in Figure 5) are nearly identical to the upstream Kuroshio water, whereas those at B1–B2 (bluish dots in Figure 5) are similar to coastal water, with low salinity ($S < 34.75$). The *T-S* properties at B3 and B4 in the Kuroshio core (reddish dots in Figure 5) are similar to each other and are considered to be representative of the Kuroshio water downstream of Seamount II. We compare *T-S* properties at B4 with those of the Kuroshio water at the mooring site. Their *T-S* properties are nearly identical in the surface ($\sigma_\theta < 23.3$) and in the deeper ($\sigma_\theta > 24.9$) layers whereas they are distinctly different in the intermediate layer.

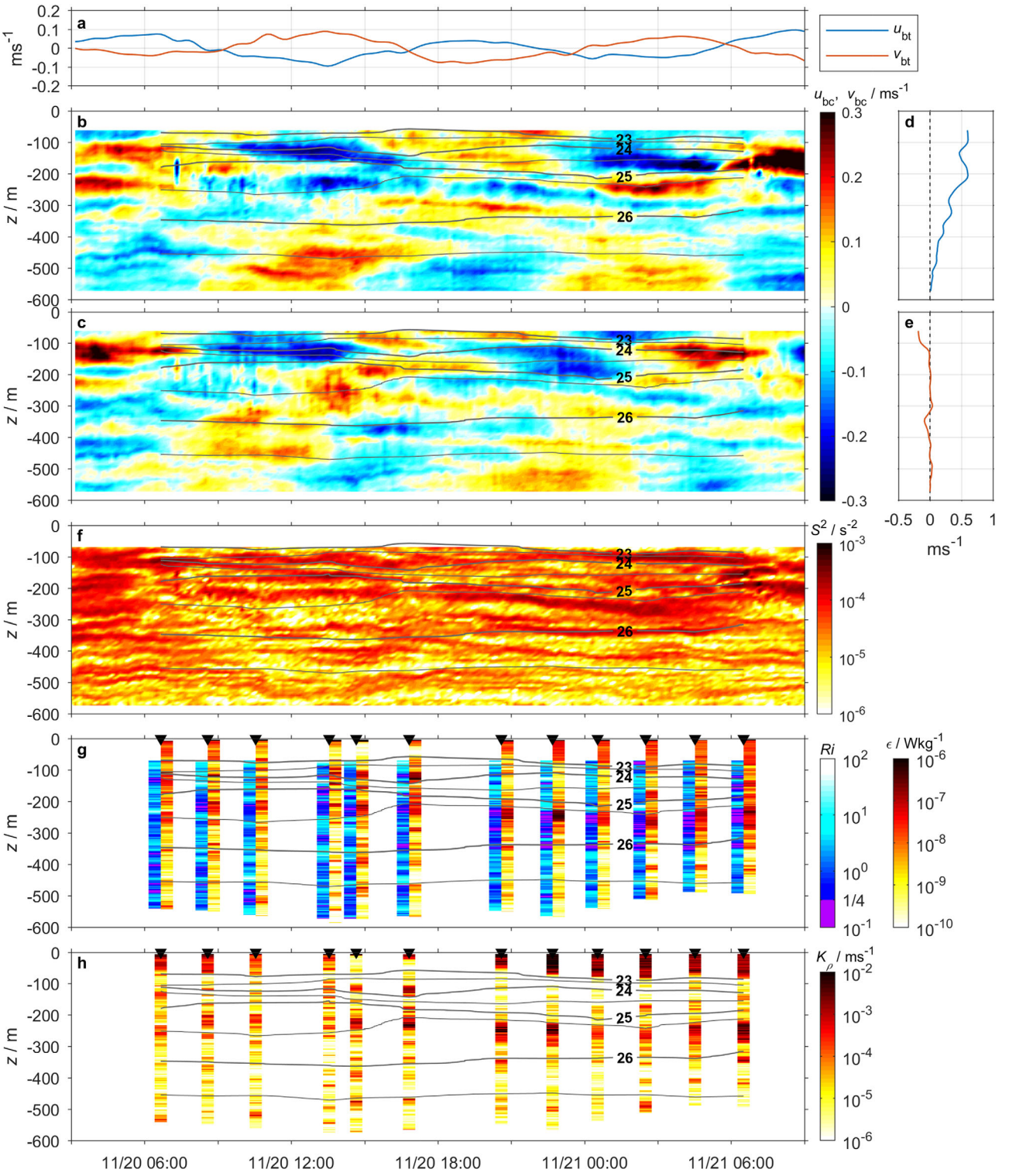

Figure 4. Time evolution of tidal currents, stratification, vertical shear and turbulence profiles at the mooring site. (a) eastward (blue) and northward (red) barotropic tidal velocities, (b) eastward and (c) northward baroclinic tidal velocities (d) time-averaged eastward and (e) northward velocity profiles (f) total vertical shear squared S^2 (g) gradient Richardson number Ri (bluish shade with purple shade indicating $Ri < 1/4$) and turbulent dissipation rate ε (reddish shade) (h) vertical eddy diffusivity K_ρ. Solid lines in Figures 4b, 4c and Figures 4f–4h represent potential density σ_θ. Horizontal axis indicates time in Japan Standard Time (JST: UTC +9 h).

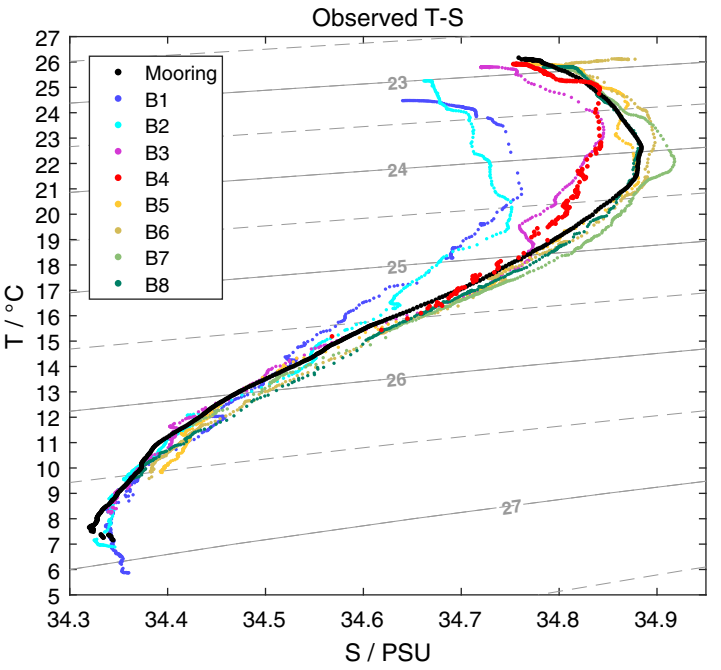

Figure 5. Temperature-salinity (*T-S*) plot from observations at the mooring site and the section B (Figure 1b): 25 h average at the mooring site (black dots), B1–B2 (bluish dots), B3–B4 (reddish dots), and B5–B8 (yellow–green dots). Contour lines indicate potential density.

The Kuroshio water at the mooring site is characterized by a subsurface salinity maximum ($S > 34.85$) existing over 100–150 m depths, one of the distinct characters of the Kuroshio in the ECS [e.g., *Yanao and Matsuno*, 2013; *Mensah et al.*, 2014]. Downstream of Seamount II (Stn.B4), the salinity maximum decreases significantly in the layer of 23.3–24.9 σ_θ. This decrease in salinity is likely due to the water-mass transformation induced by vertical mixing. The density range 23.3–24.9 σ_θ is equivalent to a depth range of 100–200 m at B4 (Figure 3, contour line) where large eddy diffusivity of $K_\rho = 2\text{–}10 \times 10^{-3}$ m^2 s^{-1} was observed (Figure 3d). Note that there is no apparent abrupt change of topography along the Kuroshio path between the mooring site and Seamount II (Figure 3). The eddy diffusivity is generally small, $K_\rho \leq O(10^{-5})$ m^2 s^{-1}, in the layer of 23.5–25.0 σ_θ at the mooring site (Figure 4d). Nevertheless, *T-S* properties drastically changed at B4. We expect that the water-mass upstream Seamount II had the same *T-S* properties as the mooring site and that most of changes in the water-mass occurs between Seamount II and B4.

To further investigate the mixing process, we considered a simple one-dimensional diffusion balance, expressed as

$$\frac{\partial T}{\partial t} = \frac{\partial}{\partial z}\left(K_T \frac{\partial T}{\partial z}\right) \qquad (1)$$

$$\frac{\partial S}{\partial t} = \frac{\partial}{\partial z}\left(K_s \frac{\partial S}{\partial z}\right)$$

where K_T and K_S are vertical eddy diffusivity of temperature and salinity, respectively. We adopt the observed eddy diffusivities at B4 and assume $K_T = K_S = K_\rho$. The observed eddy diffusivity profile is low-pass filtered in the vertical and is extrapolated using a value, $K_\rho = 1 \times 10^{-3}$ m^2 s^{-1} (shown by red line in Figure 6b) based on the observations. Note that the extrapolation does not have significant impact on the following analysis. Equations (1) are numerically integrated in time using the implicit Euler method. A second-order central difference scheme in the vertical is used to evaluate the turbulent flux divergence. Observations of the averaged *T-S* at the mooring site (black dots in Figure 5) are used as the initial condition (t = 0: black dots in Figure 6).

Figure 6a shows the temporal evolution of *T-S* properties due to the vertical divergence of turbulent fluxes. The subsurface salinity maximum at the mooring site decreases as a result of turbulent mixing. After 10 days of vertical turbulent mixing, the *T-S* properties have evolved to resemble the observed *T-S* properties at B4 (red dots in Figure 6a). The advection time scale from Seamount II to B4 is about $\Delta t_m = \Delta x/U \sim 14$ h where $\Delta x = 15$ km the distance between the seamount and B4 and $U = 0.3$ m s^{-1} the Kuroshio speed averaged over 100–200 m depths.

The much longer diffusion time scale than the advection time scale suggests that the turbulent mixing closer to Seamount II is likely at least 10 times greater than observed at B4, i.e., $K_\rho = O(10^{-2})$–$O(10^{-1})$ m^2 s^{-1}

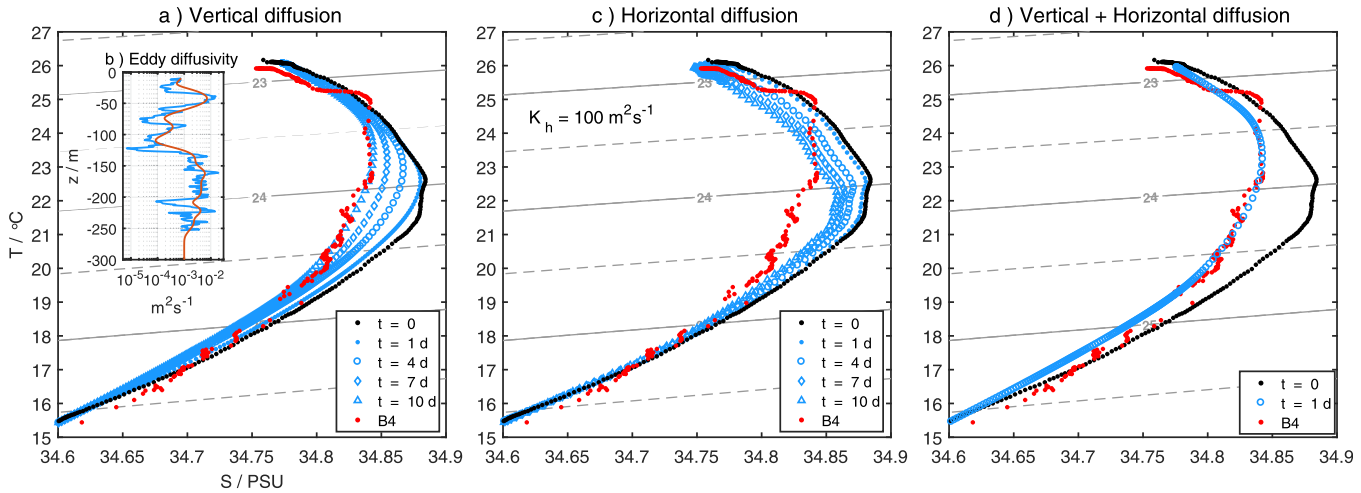

Figure 6. Examinations of *T-S* modification within the Kuroshio near Seamount II with simple diffusion models: (a) evolution of the *T-S* properties at the mooring site with the vertical diffusion based on low-pass filtered eddy diffusivity observed at B4 shown in Figure 6b: original K_ρ profile (blue) and the low-pass filtered one (red). The low-pass filtered profile is extrapolated assuming a constant value of 10^{-3} m^2 s^{-1} below 260 m depth. Different markers represent *T-S* properties at different times: t = 0 (black dots), t = 1 day (blue dots), t = 4 days (blue open circle), t = 7 days (blue open diamond), t = 10 days (blue open triangle). *T-S* at B4 is also shown by red dots. (c) Same as Figure 6a but for the horizontal diffusion with a constant horizontal eddy diffusivity, $K_h = 100$ m^2 s^{-1}. (d) *T-S* evolution at t = 1 day with combined vertical and horizontal diffusion. The vertical eddy diffusivity is 10 times larger than one used in the vertical diffusion experiment.

near Seamount II. Following *Klymak et al.* [2010], we estimate the horizontal scale of lee waves, which we believe are responsible for turbulent mixing in the vicinity of Seamount II. The horizontal wavelength of lee waves λ_x over the seamount is estimated as, $\lambda_x \sim 2\pi U_m/(\alpha N)$, where α and U_m are the topographic aspect ratio and the upstream velocity of the obstacle crest, respectively. For Seamount II where $\alpha \sim 0.1$ and $U_m \sim 1$ m s^{-1}, the estimated $\lambda_x = O(1)$ km is much shorter than $\Delta x = 15$ km, suggesting that the turbulent mixing occurs at the vicinity of the seamount. We thus speculate that the turbulent mixing near Seamount II is much more than 10 times (e.g., ~100 times) higher than the observed one at B4. Further turbulence observations and numerical experiments are needed to confirm the suggested strong turbulence near Seamount II and to understand the dynamics of the turbulent processes.

4.2. Horizontal Mixing

As discussed in the previous section, the modification of water-mass observed at B4 can be explained by vertical mixing induced by Kuroshio-topography interaction. However, lateral mixing between coastal water (B1–B2) and Kuroshio water (B5–B8) may also lead to the decrease in the salinity maximum observed at B3–B4 (Figure 5). To assess the effect, we consider horizontal diffusion between the coastal and the Kuroshio waters.

We considered the effect of horizontal mixing to the water-mass modification based on a one-dimensional horizontal diffusion equations,

$$\frac{\partial T}{\partial t} = K_h \frac{\partial^2 T}{\partial x^2}$$

$$\frac{\partial S}{\partial t} = K_h \frac{\partial^2 S}{\partial x^2} \quad (2)$$

where K_h is depth-independent horizontal eddy diffusivity. Here we consider the evolution of *T-S* properties due to horizontal mixing with coastal water (B2) and the Kuroshio water. The horizontal diffusivity K_h is set to 100 m^2 s^{-1}, following *Chang et al.* [2013] where they investigated Kuroshio-induced island wake characterized by quite similar length and velocity scales as those in the Tokara Strait. We have tested various different values of K_h, and confirmed that the conclusion of this analysis is not sensitive to varying horizontal diffusivity in its reasonable range, 1–500 m^2 s^{-1}.

Equations (2) are numerically integrated similarly as the case of the vertical diffusion. The horizontal diffusion decreases salinity of the water-mass throughout the entire depth (Figure 6c). It is obvious that at any time, the horizontal diffusion cannot explain the observed water-mass modification at B4 at all in regard to vertical profile.

We also performed a diffusion experiment with combined vertical and horizontal diffusion. Vertical and horizontal diffusivities are the same as those used for the vertical and horizontal diffusion experiments, respectively, but the former is increased by 10 times based on our speculation noted in section 4.1. The experiment reproduces the observed *T-S* properties after 1 day integration similarly as the vertical diffusion case, demonstrating the effectiveness of our speculation (Figure 6d). We thus conclude that vertical mixing plays the dominant role in modification of the Kuroshio subsurface water observed at B4 and that the contribution of lateral mixing is secondary.

5. Conclusion

This study provided evidence of strong turbulence generation in the Tokara Strait. The striking feature of the strait is that Kuroshio-topography interaction generates highly-elevated turbulence caused by many small islands and seamounts within the Kuroshio flow field. The vertical diffusivity in the Kuroshio downstream of a seamount is enhanced to $K_\rho \sim O(10^{-3})$–$O(10^{-2})$ m^2 s^{-1} in a 70 m thick elevated shear layer with $Ri < 1/4$, an increase in diffusivity of nearly 100 times from the upstream site. The observed values of K_ρ are much larger than the canonical value $K_\rho = 1 \times 10^{-4}$ m^2 s^{-1} [*Munk*, 1966; *Munk and Wunsch*, 1998] and the estimates at the margin of the ECS from the Argo floats, $K_\rho = O(10^{-5})$–$O(10^{-4})$ m^2 s^{-1} [*Whalen et al*., 2012]. The strong vertical turbulent diffusion leads to significant water-mass modification along the Kuroshio. A one-dimensional vertical diffusion model using the observed eddy diffusivity reproduces the observed water-mass transformation. However, the diffusion time scale is 10 times greater than the advection time scale from the seamount to the observed station B4, suggesting much stronger turbulent mixing occurs in the vicinity of the seamount than at B4, i.e., $K_\rho \sim O(10^{-2})$–$O(10^{-1})$ m^2 s^{-1} We also observed that at a site away from the abrupt topography, high eddy diffusivity $K_\rho \sim O(10^{-3})$ m^2 s^{-1} is related to modulation of the Kuroshio shear by internal waves motion.

An important feature of the Tokara Strait is that strong turbulent mixing is generated in the upper layer, shallower than 200 m. This is due to the presence of many shallow-water topographic features within the Kuroshio. The depth of strong vertical mixing is important for biological production; it controls nutrient supply to the euphotic zone from deeper layers. In the Kuroshio, the depth of the 1-% light intensity is usually greater than or equal to 100 m [e.g., *Shiozaki et al*., 2011]. The shallow mixing in the Tokara Strait can have impacts on high biological production there and in the downstream region [e.g., *Watanabe et al*., 1996].

Turbulent mixing induced by flow-topography interactions is generally the strongest in the area adjacent to topography [*Nikurashin and Ferrari*, 2010b; *Sheen et al*., 2013; *Alford et al*., 2013; *Nishina et al*., 2016]. *Nishina et al*. [2016] observed huge eddy diffusivity ($K_\rho \sim O(10^{-1})$ m^2 s^{-1}) in internal hydraulics in the deep Kerama Gap. *Sheen et al*. [2013] observed that locally enhanced turbulent dissipation caused by breaking lee waves radiated from rough-bottom region in the Antarctic Circumpolar Current region. The turbulence observed at B4 cannot be the decaying turbulence generated at the seamount, because the decaying time scale of turbulence is $N^{-1} \sim O(10^2)$ s, which is much shorter than the advection time scale from the Seamount II to B4, ∼1 day. We hypothesize that hydraulics and nonlinear steepening of internal lee waves lead to turbulent mixing and the associated water-mass modification. They might occur locally in the vicinity and downstream of the seamount.

Our observations revealed a feature in the Tokara Strait similar to the shear instability resulted from the blocking of the deep Kuroshio flow by a seamount east of Taiwan reported by *Chang et al*. [2016]. They reported estimation of vertical eddy diffusivities of $K_\rho \sim O(10^{-1})$ m^2 s^{-1} just above a seamount in the Kuroshio, which is consistent with our estimation. These facts suggest that the Kuroshio is strongly modified at the inlet and the outlet of the ECS. The pathway of the Kuroshio in the Tokara Strait varies on an intraseasonal time scale [*Nakamura et al*., 2006], similar to the Kuroshio east of Taiwan [*Zhang et al*., 2001]. If the Kuroshio takes the southern-mode pathway in the Tokara Strait unlike during the present observations, it may still interact effectively with steep topography associated with the Tokara Islands [*Hasegawa et al*.,

2008]. Turbulent mixing in the Tokara Strait likely depends on the Kuroshio pathway and varies on an intraseasonal time scale.

To understand turbulent mixing in the Tokara Strait, further investigations of hydraulics, generation and breaking of internal waves near the seamounts are needed. Furthermore, effects of such topographically-induced, localized turbulent mixing on modifying the total energy of the Kuroshio over the Tokara Strait remains as an open question for future studies [*Gula et al*., 2016; *Mashayek et al*., 2017]. Our study suggests that a better model prediction of the Kuroshio and water-mass properties in the Kuroshio requires an accurate parameterization of the Kuroshio interaction with topography and the associated turbulent mixing.

Acknowledgments
We would like to thank the Captain and crew of T/V *Kagoshima-maru* for their help in this field experiment and to thank Keunjong Lee, Daisuke Hasegawa, and Ayako Nishina for their help in collecting data. Bottom topography used in this study is based on the J-EGG500 produced by Japan Oceanographic Data Center (http://www.jodc.go.jp) and the ETOPO1 (http://rda.ucar.edu/datasets/ds759.4). The Kuroshio axis position data set was produced by Marine Information Research Center, Japan Hydrographical Association (http://www.mirc.jha.or.jp/en/index.html). We thank Eric D'Asaro at University of Washington for constructive comments. Comments from two anonymous reviewers are helpful in improving the original manuscript. Data used in this paper are available at https://doi.org/10.6084/m9.figshare.5135086. This study is supported by Grant-in-Aid for Scientific Research on Innovative Areas (MEXT KAKENHI grants: JP15H05821 and JP15K21710). Lien's involvement in this analysis is supported by the Office of Naval Research (N00014-15-1-2318).

References

Alford, M. H., and P. MacCready (2014), Flow and mixing in Juan de Fuca Canyon, Washington, *Geophys. Res. Lett.*, *41*, 1608–1615, doi:10.1002/2013GL058967.
Alford, M. H., et al. (2011), Energy flux and dissipation in Luzon Strait: Two tales of two ridges, *J. Phys. Oceanogr.*, *41*, 2211–2222, doi:10.1175/JPO-D-11-073.1.
Alford, M. H., J. B. Girton, G. Voet, G. S. Carter, J. B. Mickett, and J. M. Klymak (2013), Turbulent mixing and hydraulic control of abyssal water in the Samoan Passage, *Geophys. Res. Lett.*, *40*, 4668–4674, doi:10.1002/grl.50684.
Alford, M. H., et al. (2015), The formation and fate of internal waves in the South China Sea, *Nature*, *521*, 65–69.
Andres, M., M. Wimbush, J.-H. Park, K.-I. Chang, B.-H. Lim, D. R. Watts, H. Ichikawa, and W. J. Teague (2008), Observations of Kuroshio flow variations in the East China Sea, *J. Geophys. Res.*, *113*, C05013, doi:10.1029/2007JC004200.
Andres, M., S. Jan, T. B. Sanford, V. Mensah, L. R. Centurioni, and J. W. Book (2015), Mean structure and variability of the Kuroshio from northeastern Taiwan to southwestern Japan, *Oceanography*, *28*, 84–95, doi:10.5670/oceanog.2015.84.
Baines, P. G. (1995), *Topographic Effects in Stratified Flows*, 482 pp., Cambridge Univ. Press, Cambridge, U. K.
Chang, M.-H., T. Y. Tang, C.-R. Ho, and S.-Y. Chao (2013), Kuroshio-induced wake in the lee of Green Island off Taiwan, *J. Geophys. Res. Oceans*, *118*, 1508–1519, doi:10.1002/jgrc.20151.
Chang, M.-H., S.-Y. Jheng, and R.-C. Lien (2016), Trains of large Kelvin-Helmholtz billows observed in the Kuroshio above a seamount, *Geophys. Res. Lett.*, *43*, 8654–8661, doi:10.1002/2016GL069462.
Dillon, T. M. (1982), Vertical overturns: A comparison of Thorpe and Ozmidov length scales, *J. Geophys. Res.*, *87*, 9601–9613.
Feng, M., H. Mitsudera, and Y. Yoshikawa (2000), Structure and variability of the Kuroshio current in Tokara Strait, *J. Phys. Oceanogr.*, *30*, 2257–2276.
Gregg, M. C., and J. M. Klymak (2014), Mode-2 hydraulic control of flow over a small ridge on a continental shelf, *J. Geophys. Res. Oceans*, *119*, 8093–8108, doi:10.1002/2014JC010043.
Gula, J., M. J. Molemaker, and J. C. McWilliams (2016), Topographic generation of submesoscale centrifugal instability and energy dissipation, *Nat. Commun.*, *7*, 1–7.
Guo, X., X.-H. Zhu, Q.-S. Wu, and D. Huang (2012), The Kuroshio nutrient stream and its temporal variation in the East China Sea, *J. Geophys. Res.*, *117*, C01026, doi:10.1029/2011JC007292.
Guo, X. Y., X.-H. Zhu, Y. Long, and D. J. Huang (2013), Spatial variations in the Kuroshio nutrient transport from the East China Sea to south of Japan, *Biogeosciences*, *10*, 6403–6417, doi:10.5194/bg-10-6403-2013.
Hasegawa, D., H. Yamazaki, T. Ishimaru, H. Nagashima, and Y. Koike (2008), Apparent phytoplankton bloom due to island mass effect, *J. Mar. Syst.*, *69*, 238–246.
James, C., M. Wimbush, and H. Ichikawa (1999), Kuroshio meanders in the East China Sea, *J. Phys. Oceanogr.*, *29*, 259–272.
Jan, S., R.-C. Lien, and C.-H. Ting (2008), Numerical study of baroclinic tides in Luzon Strait, *J. Oceanogr.*, *64*, 789–802.
Kerry, C. G., B. S. Powell, and G. S. Carter (2014), The impact of subtidal circulation on internal tide generation and propagation in the Philippine Sea, *J. Phys. Oceanogr.*, *44*, 1386–1405, doi:10.1175/JPO-D-13-0142.1.
Kida, S., et al. (2015), Oceanic fronts and jets around Japan: A review, *J. Oceanogr.*, *71*, 469–497.
Klymak, J. M., and M. C. Gregg (2004), Tidally generated turbulence over the Knight Inlet sill, *J. Phys. Oceanogr.*, *34*, 1135–1151.
Klymak, J. M., S. Legg, and R. Pinkel (2010), High-mode stationary waves in stratified flow over large obstacles, *J. Fluid Mech.*, *644*, 321–336.
Klymak, J. M., M. H. Alford, R. Pinkel, R.-C. Lien, Y.-J. Yang, and T.-Y. Tang (2011), The breaking and scattering of the internal tide on a continental slope, *J. Phys. Oceanogr.*, *41*, 926–945, doi:10.1175/2010JPO4500.1.
Kodama, T., Y. Shimizu, T. Ichikawa, Y. Hiroe, A. Kusaka, H. Morita, M. Shimizu, and K. Hidaka (2014), Seasonal and spatial contrast in the surface layer nutrient content around the Kuroshio along 138°E, observed between 2002 and 2013, *J. Oceanogr.*, *70*, 489, doi:10.1007/s10872-014-0245-5.
Legg, S., and J. Klymak (2008), Internal hydraulic jumps and overturning generated by tidal flow over a tall steep ridge, *J. Phys. Oceanogr.*, *38*, 1949–1964.
Lien, R.-C., T. B. Sanford, and S. Jan (2013), Internal tides on East China Sea continental slope, *J. Mar. Res.*, *71*, 151–186.
Lien, R.-C., et al. (2015), The Kuroshio and Luzon Undercurrent east of Luzon Island, *Oceanography*, *28*, 54–63.
Liu, K.-K., C.-K. Kang, T. Kobari, H. Liu, C. Rabouille, and K. Fennel (2014), Biogeochemistry and ecosystems of continental margins in the western North Pacific Ocean and their interactions and responses to external forcing – an overview and synthesis, *Biogeosciences*, *11*, 7061–7075, doi:10.5194/bg-11-7061-2014.
Mashayek, A., R. Ferrari, S. Merrifield, J. R. Ledwell, L. St. Laurent, and A. Naveira Garabato (2017), Topographic enhancement of vertical turbulent mixing in the Southern Ocean, *Nat. Commun.*, *8*, 1–12.
Matsuno, T., M. Simizu, Y. Morii, H. Nishida, and Y. Takagi (2005), Measurements of the turbulent energy dissipation rate around the shelf break in the East China Sea, *J. Oceanogr.*, *61*, 1029–1037.
Mensah, V., S. Jan, M.-D. Chiou, T.-H. Kuo, and R.-C. Lien (2014), Evolution of the Kuroshio tropical water from the Luzon Strait to the east of Taiwan, *Deep Sea Res., Part I*, *86*, 68–81.
Mohri, K., T. Hibiya, and N. Iwamae (2010), Revisiting internal wave generation by tide-topography interaction, *J. Geophys. Res.*, *115*, C11001, doi:10.1029/2009JC005908.
Munk, W. (1966), Abyssal recipes, *Deep Sea Res. Oceanogr. Abstr.*, *13*, 707–730.

Munk, W., and C. Wunsch (1998), Abyssal recipes II: Energetics of tidal and wind mixing, *Deep Sea Res., Part I*, *45*, 1977–2010.
Nagai, T., A. Tandon, E. Kunze, and A. Mahadevan (2015), Spontaneous generation of near-inertial waves by the Kuroshio Front, *J. Phys. Oceanogr.*, *45*, 2381–2406.
Nakamura, H., H. Ichikawa, A. Nishina, and H.-J. Lie (2003), Kuroshio path meander between the continental slope and the Tokara Strait in the East China Sea, *J. Geophys. Res.*, *108*(C11), 3360, doi:10.1029/2002JC001450.
Nakamura, H., T. Yamashiro, A. Nishina, and H. Ichikawa (2006), Time-frequency variability of Kuroshio meanders in Tokara Strait, *Geophys. Res. Lett.*, *33*, L21605. doi:10.1029/2006GL027516.
Nakamura, H., A. Nishina, and S. Minobe (2012), Response of storm tracks to bimodal Kuroshio path states south of Japan, *J. Clim.*, *25*, 7772–7779, doi:10.1175/JCLI-D-12-00326.1.
Nakamura, H., A. Nishina, Z. Liu, F. Tanaka, M. Wimbush, and J.-H. Park (2013), Intermediate and deep water formation in the Okinawa Trough, *J. Geophys. Res. Oceans*, *118*, 6881–6893, doi:10.1002/2013JC009326.
Nakamura, T., Y. Isoda, H. Mitsudera, S. Takagi, and M. Nagasawa (2010), Breaking of unsteady lee waves generated by diurnal tides, *Geophys. Res. Lett.*, *37*, L04602, doi:10.1029/2009GL041456.
Nasmyth, P. W. (1970), Oceanic turbulence, PhD dissertation, 109 pp., Univ. of B. C,. Vancouver, Canada.
Nikurashin, M., and R. Ferrari (2010a), Radiation and dissipation of internal waves generated by geostrophic motions impinging on small-scale topography: Theory, *J. Phys. Oceanogr.*, *40*, 1055–1074.
Nikurashin, M., and R. Ferrari (2010b), Radiation and dissipation of internal waves generated by geostrophic flows impinging on small-scale topography: Application to the Southern Ocean, *J. Phys. Oceanogr.*, *40*, 2025–2042.
Nishina, A., H. Nakamura, J.-H. Park, D. Hasegawa, Y. Tanaka, S. Seo, and T. Hibiya (2016), Deep ventilation in the Okinawa Trough induced by Kerama Gap overflow, *J. Geophys. Res. Oceans*, *121*, 6092–6102, doi:10.1002/2016JC011822.
Niwa, Y., and T. Hibiya (2004), Three-dimensional numerical simulation of M2 internal tides in the East China Sea, *J. Geophys. Res.*, *109*, C04027, doi:10.1029/2003JC001923.
Oka, E., and M. Kawabe (2003), Dynamic structure of the Kuroshio south of Kyushu in relation to the Kuroshio path variations, *J. Oceanogr.*, *59*, 595–608.
Osborn, T. (1980), Estimates of the local rate of vertical diffusion from dissipation measurements, *J. Phys. Oceanogr.*, *10*, 83–89.
Rainville, L., and R. Pinkel (2004), Observations of energetic high-wavenumber internal waves in the Kuroshio, *J. Phys. Oceanogr.*, *34*, 1495–1505.
Rainville, L., C. M. Lee, D. L. Rudnick, and K.-C Yang (2013), Propagation of internal tides generated near Luzon Strait: Observations from autonomous gliders, *J. Geophys. Res. Oceans*, *118*, 4125–4138, doi:10.1002/jgrc.20293.
Sheen, K. L., et al. (2013), Rates and mechanisms of turbulent dissipation and mixing in the Southern Ocean: Results from the Diapycnal and Isopycnal Mixing Experiment in the Southern Ocean (DIMES), *J. Geophys. Res. Oceans*, *118*, 2774–2792, doi:10.1002/jgrc.20217.
Shiozaki, T., K. Furuya, H. Kurotori, T. Kodama, S. Takeda, T. Endoh, Y. Yoshikawa, J. Ishizaka, and T. Matsuno (2011), Imbalance between vertical nitrate flux and nitrate assimilation on a continental shelf: Implications of nitrification, *J. Geophys. Res.*, *116*, C10031, doi:10.1029/2010JC006934.
St. Laurent, L. C., and A. M. Thurnherr (2007), Overflow mixing of lower thermocline water on the crest of the Mid-Atlantic Ridge, *Nature*, *448*, 680–683, doi:10.1038/nature06043.
Thorpe, S. (1977), Turbulence and mixing in a Scottish loch, *Philos. Trans. R. Soc. London A*, *286*, 125–181.
Tsutsumi, E., and X. Guo (2016), Climatology and linear trends of seasonal water temperature and heat budget in a semienclosed sea connected to the Kuroshio region, *J. Geophys. Res. Oceans*, *121*, 4649–4669, doi:10.1002/2016JC011748.
Varlamov, S. M., X. Guo, T. Miyama, K. Ichikawa, T. Waseda, and Y. Miyazawa (2015), M2 baroclinic tide variability modulated by the ocean circulation south of Japan, *J. Geophys. Res. Oceans*, *120*, 3681–3710, doi:10.1002/2015JC010739.
Watanabe, Y., H. Zentani, and R. Kimura (1996), Offshore expansion of spawning of the Japanese sardine, Sardinops melanostictus, and its implication for egg and larval survival, *Can. J. Fish. Aquat. Sci.*, *53*, 55–61.
Waterman, S., A. C. Naveira-Garabato, and K. L. Polzin (2013), Internal waves and turbulence in the Antarctic Circumpolar Current, *J. Phys. Oceanogr.*, *43*, 259–282, doi:10.1175/JPO-D-11-0194.1.
Whalen, C. B., L. D. Talley, and J. A. MacKinnon (2012), Spatial and temporal variability of global ocean mixing inferred from Argo profiles, *Geophys. Res. Lett.*, *39*, L18612, doi:10.1029/2012GL053196.
Yanao, S., and T. Matsuno (2013), Characteristics of outer shelf water in the East China Sea, *J. Oceanogr.*, *69*, 245–258.
Zhang, D., T. N. Lee, W. E. Johns, C.-T. Liu, and R. Zantopp (2001), The Kuroshio east of Taiwan: Modes of variability and relationship to interior ocean mesoscale eddies, *J. Phys. Oceanogr.*, *11*, 1054–1074.